First simultaneous space measurements of atmospheric pollutants in the boundary layer from IASI: A case study in the North China Plain

Anne Boynard, Cathy Clerbaux, Lieven Clarisse, Sarah Safieddine, Matthieu Pommier, Martin van Damme, Sophie Bauduin, Charlotte Oudot, Juliette Hadji-Lazaro, Daniel Hurtmans, et al.

AGU PUBLICATIONS

Geophysical Research Letters

RESEARCH LETTER
10.1002/2013GL058333

Key Points:
- IASI is suitable to monitor high anthropogenic pollution over China
- Stable meteorological conditions favor detection of boundary layer pollutants
- High CO, SO2, NH3, and ammonium sulfate aerosol are measured in January 2013

Supporting Information:
- Readme
- Figure S1
- Figure S2
- Figure S3

Corresponding to:
A. Boynard,
anne.boynard@latmos.ipsl.fr

Citation:
Boynard, A., et al. (2014), First simultaneous space measurements of atmospheric pollutants in the boundary layer from IASI: A case study in the North China Plain, *Geophys. Res. Lett.*, *41*, 645–651, doi:10.1002/2013GL058333.

Received 15 OCT 2013
Accepted 9 DEC 2013
Accepted article online 12 DEC 2013
Published online 17 JAN 2014

First simultaneous space measurements of atmospheric pollutants in the boundary layer from IASI: A case study in the North China Plain

Anne Boynard[1], Cathy Clerbaux[1,2], Lieven Clarisse[2], Sarah Safieddine[1], Matthieu Pommier[1,3], Martin Van Damme[2,4], Sophie Bauduin[2], Charlotte Oudot[1], Juliette Hadji-Lazaro[1], Daniel Hurtmans[2], and Pierre-Francois Coheur[2]

[1]UPMC Université Paris 6, Université Versailles St.-Quentin, CNRS-INSU, LATMOS-IPSL, Paris, France, [2]Spectroscopie de l'atmosphère, Chimie Quantique et Photophysique, Université Libre de Bruxelles, Brussels, Belgium, [3]Université Versailles St-Quentin, UMR 8212, CEA-CNRS-UVSQ, LSCE-IPSL, CEA Saclay, Gif-sur-Yvette, France, [4]Earth and Climate Cluster, Department of Earth Sciences, Vrije Universiteit Amsterdam, Amsterdam, Netherlands

Abstract In this paper we investigate a severe pollution episode that occurred in Beijing, Tianjin, and the Hebei province in January 2013. The episode was caused by the combination of anthropogenic emissions and a high-pressure system that trapped pollutants in the boundary layer. Using IASI (Infrared Atmospheric Sounding Interferometer) satellite measurements, high concentrations of key trace gases such as carbon monoxide (CO), sulfur dioxide (SO_2), and ammonia (NH_3) along with ammonium sulfate aerosol ($(NH_4)_2SO_4$) are found. We show that IASI is able to detect boundary layer pollution in case of large negative thermal contrast combined with high levels of pollution. Our findings demonstrate that anthropogenic key pollutants, such as CO and SO_2, can be monitored by IASI in the North China Plain during wintertime in support of air quality evaluation and management.

1. Introduction

Air pollution is a major issue in China's urban and industrial centers [*Zhang et al.*, 2008] due to the expansion of industrialization (e.g., power plants, industrial production, and transportation), economic growth, and the important growth in car ownership. Coal burning, which is a major source of carbon monoxide (CO), sulfur dioxide (SO_2), and particulate matter (PM), is the main source of air pollution in China, accounting for more than 70% of its total energy consumption [*National Bureau of Statistics of China*, 2008]. SO_2 emissions contribute to acid deposition [*Schwartz*, 1989] and can affect air quality and climate through the formation of sulfate aerosols [e.g., *Liu et al.*, 2008]. In winter, emissions related to domestic heating are an important source of CO in China. Due to its medium tropospheric lifetime (weeks to months), CO is a useful tracer for atmospheric pollution transport [e.g., *Edwards et al.*, 2006]. CO is also a key pollutant in global atmospheric chemistry since its oxidation is the main sink of OH radicals [*Warneck*, 2000]. Also, it contributes importantly to air quality degradation in most of the cities of the developing world. Ammonia (NH_3), largely emitted from agriculture and synthetic fertilizer production [e.g., *Bouwman et al.*, 1997], constitutes another important source of pollution in China [*Huang et al.*, 2012], leading to the formation of secondary aerosols such as ammonium sulfate ($(NH_4)_2SO_4$).

Although many efforts have been made to improve air quality in China, pollution still often occurs in urban and surrounding areas during both summertime and wintertime [e.g., *Wang et al.*, 2006; *Zhao et al.*, 2013]. The North China Plain, including Beijing, Tianjin, and the Hebei (BTH) province, is one of the most severely polluted areas in the world [*van Donkelaar et al.*, 2010]. During the first 2 weeks of January 2013, the North China Plain faced an extreme air pollution episode, raising considerable public attention. Beijing and many other cities were affected by a persistent haze [*Wang et al.*, 2013], leading to a significant increase of respiratory illness [e.g., *Hu*, 2009], with a visibility down to 100 m. Such pollution events generally occur in winter, when anthropogenic pollutants accumulate over the North China Plain due to weather conditions [*Li et al.*, 2011]. During winter, this region is often dominated by a cold high-pressure system generating less wind, sometimes also accompanied by surface temperature inversions leading to weak mixing and dispersion [*Xu et al.*, 2011].

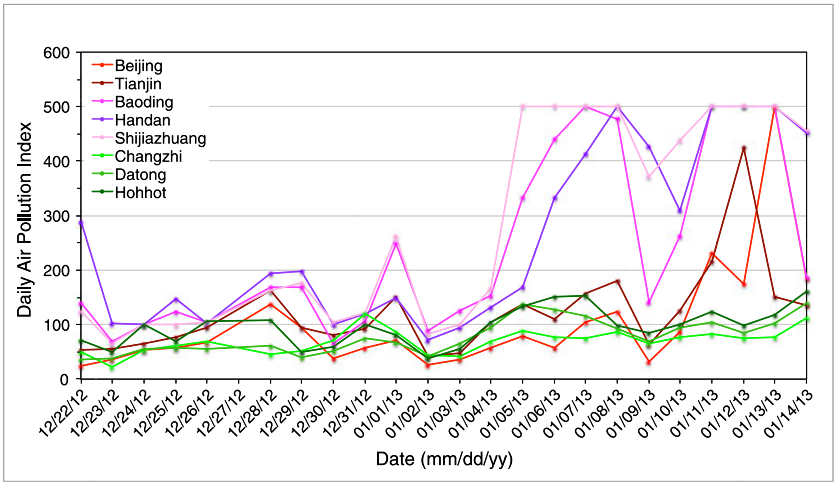

Figure 1. Daily Air Pollution Index (DAPI) from highly urbanized industrial (purple/red color) and remote cities (green colors) located in Beijing, Tianjin, and the Hebei province in the North China Plain. The air quality in highly urbanized industrial cities decreases from 5 to 14 January 2013, which is attributed to the buildup of pollution due to the combination of anthropogenic emissions and stable meteorological conditions. Values can be found at http://datacenter.mep.gov.cn.

The Infrared Atmospheric Sounding Interferometer (IASI) [*Clerbaux et al.*, 2009] is a nadir-viewing spectrometer launched on board the European MetOp-A (Meteorological Operational A) platform in 2006. IASI measures the thermal infrared (TIR) radiation emitted from the surface of the Earth and the atmosphere in the spectral range extending from 645 to 2760 cm^{-1}. Global coverage is achieved twice a day (at 09:30 and 21:30 local solar time) with a 12 km diameter field of view at nadir. The combination of its excellent temporal and spatial coverage along with its high spectral resolution and instrumental characteristics makes IASI one of the most advanced onboard instruments able to monitor a suite of atmospheric trace gases [including CO, ozone (O_3), nitric acid (HNO_3), SO_2, NH_3] as well as to detect the evolution of atmospheric plumes from volcanic, biomass burning, and anthropogenic origin [e.g., *Turquety et al.*, 2009; *Clarisse et al.*, 2011]. Infrared sounders are commonly known to have higher sensitivity in the free troposphere (FT) and limited or no sensitivity in the lower troposphere. However, this latter statement is oversimplified, as the sensitivity of such instruments depends on different factors: the target species, instrumental noise, spectral resolution, and thermal contrast (this is the temperature difference between the surface and the air above it) [*Clarisse et al.*, 2010]. Previous studies have shown that high thermal contrast favors the infrared detection of trace gases in the lower troposphere, such as CO [*Deeter et al.*, 2007] or NH_3, a short-lived species, emitted at the surface [*Clarisse et al.*, 2010].

In this paper we analyze a severe winter pollution episode that occurred in the North China Plain in January 2013 using IASI measurements. For this event, IASI was able to measure anthropogenic plume enhancements of four major air pollutants: CO, SO_2, NH_3, and $(NH_4)_2SO_4$.

2. The January Severe Pollution Event and IASI Satellite Measurements

The meteorological conditions are analyzed using ECMWF (European Center for Medium-Range Weather Forecasts) Re-Analysis (ERA). The data assimilation produces four analyses per day at 00:00, 06:00, 12:00, and 18:00 UTC with a Gaussian grid with a resolution of 0.7° at the equator. Data services apply an interpolation scheme to make it adaptable to requested resolutions and representation forms [*Berrisford et al.*, 2009; *Dee et al.*, 2011]. In the ERA-Interim database, the data are interpolated and extracted over a grid size of 0.75° × 0.75°. The nighttime reanalysis shows that the BTH area was characterized by low surface wind speeds (which are generally lower than 3 m s^{-1}) and stable atmospheric conditions [planetary boundary layer (PBL) height mainly lower than 100 m] during the 3–13 January period, which prevents the dispersion of pollutants. Figure S1 shows the time series of wind speed and PBL height obtained from ECMWF reanalysis for a few selected highly polluted cities during the first half of January. These stagnant conditions led to the buildup of pollutant concentrations as revealed in the strong increase of the Daily Air Pollution Index (DAPI) [*Gao et al.*, 2011] of several highly urbanized industrial cities in the BTH area during the 5–14 January period (see Figure 1). DAPI values over 500 were found in several major industrial cities such as Baoding, Handan, and

Shijiazhuang over several days. In Beijing, the index steadily increased to reach the 500 saturation level on 13 January. The DAPI level is also shown for some cities not affected by the pollution (Changzhi, Datong, and Hohhot), where it is characterized by values generally lower than 100. The DAPI level is defined as the highest level of pollutant among six atmospheric pollutants measured by the monitoring stations in each city: SO_2, NO_2, PM2.5, PM10 (2.5 and 10 μm diameter particulate matters, respectively), CO, and O_3. For this pollution event, the highest value of the six air pollutants was the PM value (cf. http://datacenter.mep.gov.cn/report/air_daily).

Transport of pollution was investigated with the online Hybrid Single-Particle Lagrangian Integrated Trajectory (HYSPLIT) model [*Draxler and Rolph*, 2014]. HYSPLIT was run over 5 days with altitudes ranging from the surface to 3000 m in a 0.2° × 0.2° box around several highly polluted cities in the BTH area. The run was driven by the National Centers for Environmental Prediction reanalysis. The trajectory calculations show that the air mass was localized in the BTH province, indicating that the pollution was not due to transport but to local anthropogenic emissions and production of secondary pollutants.

To better understand the source of this pollution episode, we analyzed IASI measurements for several major air pollutants: CO, O_3, SO_2, NH_3, and $(NH_4)_2SO_4$. No enhancement of IASI tropospheric O_3 was observed during this winter pollution episode. This can be linked to the slow photochemical activity in winter along with the long O_3 lifetime in midlatitude winter and to the complexity of O_3 production that depends on the availability of its precursors [*Lelieveld and Dentener*, 2000]. Also, the IASI daytime overpasses were not ideal because of interfering clouds, especially from 7 to 13 January (when high levels of pollution were reported). Therefore, only the nighttime measurements were used in this study. IASI CO retrievals are based on the optimal estimation scheme (OEM) described by *Rodgers* [2000] and were performed only for pixels with a cloud coverage below 25%. For SO_2, the method follows the OEM development made in *Carboni et al.* [2012], which allows better sensitivity due to the use of a wide spectral range (more information) and a dedicated spectral measurement variance-covariance matrix (more variability allowed) [see also *Bauduin et al.*, 2013]. The NH_3 retrieval scheme consists of the calculation of a dimensionless hyperspectral index using an extended spectral range (800–1200 cm^{-1}), which is subsequently converted to a total NH_3 column using look-up tables built from forward radiative transfer model simulations [*Van Damme et al.*, 2013]. We refer to other studies for a full description of the retrieval details, namely, *Hurtmans et al.* [2012] for CO, *Bauduin et al.* [2013] for SO_2, and *Van Damme et al.* [2013] for NH_3. Note that fog formation is quite common over the BTH area at this time of the year and can have an impact on the retrievals. A quantitative analysis of their effect on the satellite retrievals is out of the scope of this study, but in general, they could yield an underestimation of the retrieved products.

The first observations of $(NH_4)_2SO_4$ from IASI were reported in *Clarisse et al.* [2013] within a more general framework of aerosol detection and type speciation using infrared measurements. For $(NH_4)_2SO_4$, the detection is mainly based on the calculation of an index (hereinafter R_N; see *Clarisse et al.* [2013] for details), which is a measure of the aerosol signal strength in the spectrum. Under constant atmospheric conditions, this quantity correlates with the column amount. At present, rigorous quantification of $(NH_4)_2SO_4$ from IASI spectra has, however, not been attempted as signal strengths are very small, and as such, quantification requires making assumptions on composition and size distribution.

The time series of IASI CO total column retrievals averaged over a 0.5° × 0.5° box around each selected city (see Figure S2) is consistent with that of DAPI (see Figure 1). The CO concentrations range from 4×10^{18} to 10×10^{18} molecules cm^{-2} in major highly urbanized industrial and coal-burning sectors in Tianjin and the Hebei province, as well as in Beijing, starting from 4 January. Lower concentrations of CO ($<2 \times 10^{18}$ molecules cm^{-2}) were observed by IASI in remote cities, which is in agreement with the low DAPI levels. Note that for a few days (e.g., 5 January), the CO and DAPI values do not correlate, which is due to a less favorable thermal contrast.

3. PBL Pollution as Observed by IASI

A more detailed analysis of the IASI retrievals is presented hereinafter for the 12 January case, when the largest plume of CO was observed by IASI. Figures 2a and 2b show the spatial distribution of CO total column retrievals on 12 January 2013 (nighttime) and the corresponding number of independent pieces of information on the vertical profile [or degrees of freedom for signal (DOFS)] [*Rodgers*, 2000], respectively. The plots show that clear enhancement of CO is observed in the BTH area, with concentrations varying from 4×10^{18} to 10×10^{18} molecules cm^{-2} and total DOFS values within the plume ranging from 1.3 to 1.7. By examining the

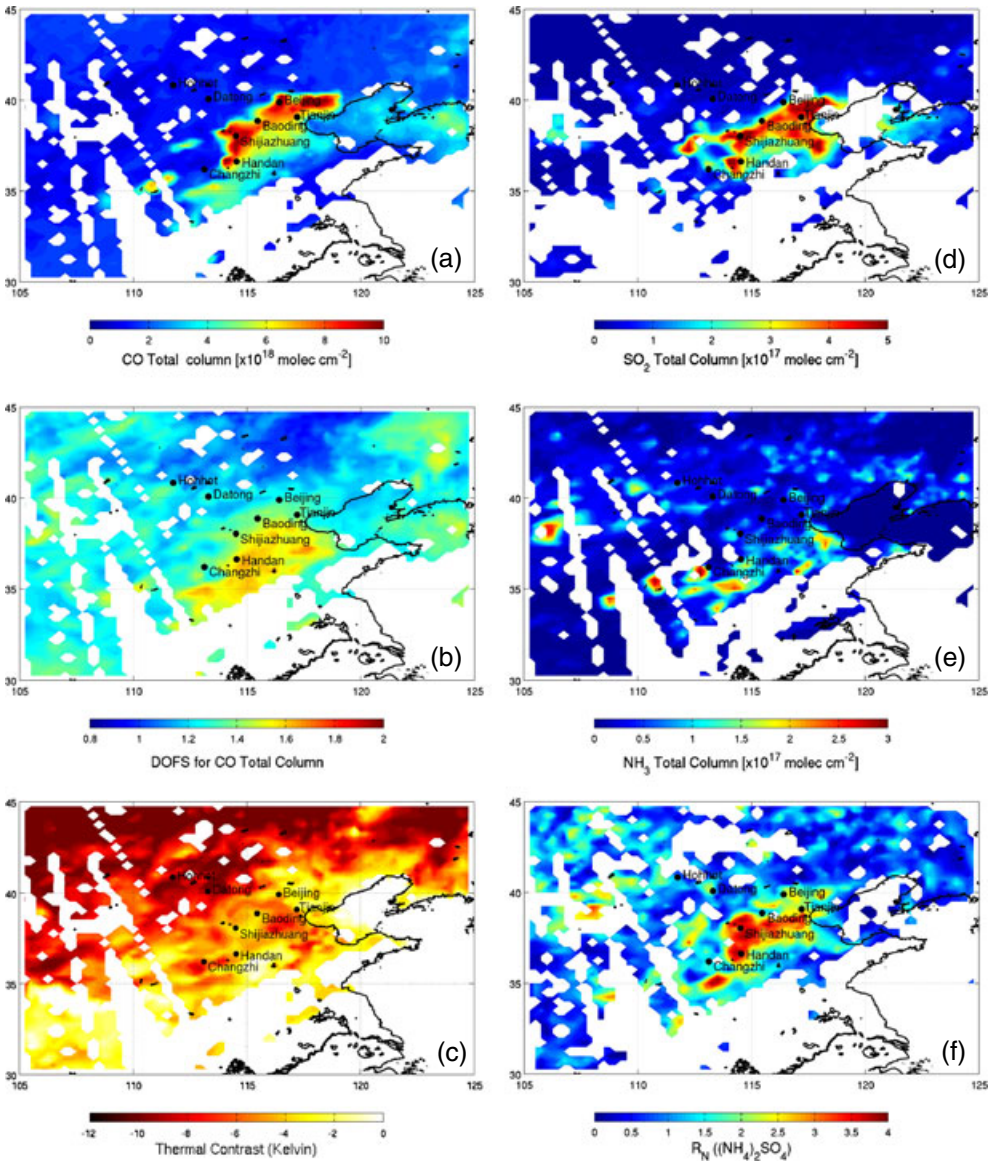

Figure 2. Spatial distributions of IASI nighttime observations on 12 January 2013: (a) CO total column, (b) total degrees of freedom for signal (DOFS) characterizing the CO total column retrievals, (c) thermal contrast, (d) SO_2 total column, (e) NH_3 total column, and (f) ammonium sulfate aerosol in terms of R_N. All data are interpolated on a 0.25° × 0.25° grid. The white areas correspond to no data.

averaging kernels (AKs) within the plume (see example in Figure S3), we clearly see that the AK row for surface CO peaks at the surface, which is mainly associated with the presence of a large negative thermal contrast (−10 K). Furthermore, the AK row for surface CO peaks more at the surface than in the FT, indicating that IASI measurements are more sensitive to the surface than to the FT. This shows the IASI ability to monitor PBL CO in the North China Plain in winter. Besides, the analysis of the error budget within the plume indicates a total error (including measurement and smoothing errors) lower than 10% in the PBL.

Figures 2d–2f illustrate the spatial distributions of IASI SO_2 and NH_3 total columns and the qualitative R_N measure for $(NH_4)_2SO_4$ aerosols, respectively, for 12 January. Comparison of SO_2 and CO retrievals reveals coincident enhancements located in Beijing, as well as in Tianjin and the Hebei province, with a mean daily SO_2 concentration of 6.9 ± 6.3 Dobson unit (DU) in the Beijing area. As shown in Figure 2c, thermal contrast is mainly negative, which means that boundary layer species emit more radiation than they absorb, giving rise to emission signatures in the observed spectra. Observing these for pollutants such as SO_2 or NH_3 implies the presence of enhanced loadings of these species in a boundary layer with temperature

Table 1. IASI SO_2 and CO Total Columns and Surface Mixing Ratios Averaged Over a 2°× 2° Box Centered in Beijing for the Winter Season and Comparisons With Literature Data[a]

		Mean ± SD	
SO_2 Measurements	Time	TC (DU)	VMR (ppbv)
IASI [this work]	12 Jan	6.9 ± 6.3	60 ± 55
IASI [this work]	Dec–Jan (DJ) 2013	3.3 ± 4.2	28 ± 38
OMPS [*Yang et al.*, 2013]	Jan 2013	~1.5[b]	
OMI [*Yang et al.*, 2013]	DJ 2013	~1.0[c]	
SCIAMACHY [*Zhang et al.*, 2012]	Jan 2004–2009	~0.8[d]	
In situ [*Lin et al.*, 2012]	Jan 2007–2010		41 ± 8
In situ [*Lin et al.*, 2011]	Nov 2007 to Mar 2008		32 ± 2
In situ [*Li et al.*, 2011]	Nov 2009 (hazy-only days)		83
In situ [*Xu et al.*, 2011]	DJ 2010		29 ± 23
		Mean ± SD	
CO Measurements	Time	TC ($\times 10^{17}$ molecules cm^{-2})	VMR (ppmv)
IASI [this work]	12 Jan	44 ± 35	1.4 ± 1.3
IASI [this work]	DJ 2013	26 ± 20	0.5 ± 0.8
MOPITT [this work]	DJ 2013	24 ± 7	0.1 ± 0.06
In situ [*Lin et al.*, 2011]	Nov 2007 to Mar 2008		1.99 ± 0.13
In situ [*Li et al.*, 2011]	Nov 2009 (hazy-only days)		2.1

[a]The standard deviation (SD) is also indicated.
[b]Estimated from *Yang et al.* [2013, Figure 3a].
[c]Estimated from *Xu et al.* [2011, Figure 4c].
[d]Estimated from *Zhang et al.* [2012, Figure 2a].

inversion or large thermal contrasts [*Clarisse et al.*, 2010; *Bauduin et al.*, 2013; *Van Damme et al.*, 2013]. Current studies have shown that the IASI measurement of anthropogenic SO_2 in the PBL is facilitated when a combination of persisting high pollution with high negative thermal contrast and low surface humidity occurs, such as, e.g., over Norilsk (Siberia) throughout wintertime [*Bauduin et al.*, 2013].

A statistical analysis on IASI SO_2 and CO total columns along with surface mixing ratio retrievals averaged over a 2° × 2° box centered in Beijing is summarized in Table 1. A comparison with available literature data for the winter season and the same region is also presented. The monthly average SO_2 concentration is 3.3 ± 4.2 DU, which is 2–3 times higher than those estimated from other satellite measurements [*Yang et al.*, 2013; *Zhang et al.*, 2012]. Our retrieved values might be somewhat overestimated by the use of level 2 temperature profile and surface temperature that underestimates the thermal contrast. At the surface, the monthly mean IASI SO_2 mixing ratio (28 ppbv) is very close to those calculated from in situ measurements in the Beijing area [*Lin et al.*, 2011, 2012; *Xu et al.*, 2011]. On 12 January when the pollution peaked, the mean IASI SO_2 mixing ratio is similar to the values reported by *Li et al.* [2011] for hazy-only days (60 ppbv versus 83 ppbv, respectively). Regarding CO retrievals, the mean monthly IASI CO surface mixing ratio is 0.5 ± 0.8 ppmv in the Beijing area, which is 4 times lower than those estimated from in situ measurements [*Lin et al.*, 2011; *Xu et al.*, 2011]. Although the IASI CO retrieved values might be underestimated at the surface, possibly due to a limited sensitivity, we show that in the presence of large negative thermal contrast combined with high levels of pollution, anthropogenic CO mixing ratio can be detected from space in the PBL. In addition, the mean IASI CO mixing ratio is in good agreement with the mean CO mixing ratio retrieved from MOPITT (Measurements of Pollution in the Troposphere) measurements in the same region [*Xu et al.*, 2011]. This indirect validation with correlative satellite and in situ observations shows the performance of IASI to measure SO_2 and CO in the PBL.

High concentrations of NH_3 were also observed (values up to 3×10^{17} molecules cm^{-2}), especially in the south of Hebei province dominated by intensive agriculture local source areas. The NH_3 hot spots were not found at the same location as CO and SO_2, which is expected as NH_3 is emitted mainly from agriculture and farming practices. As shown by *Van Damme et al.* [2013], errors associated with NH_3 total columns can be high during the night (mostly above 75%) when surface sensitivity is reduced. However, during this pollution event, errors in the range of 60–75% are found within the NH_3 plumes, which is associated with the presence of temperature inversions in the PBL favoring a higher sensitivity toward the surface.

Ammonium sulfates, which represent a major part of anthropogenic aerosols, were detected with confidence, and the plume coincides very well with the increase in CO and SO_2. The $(NH_4)_2SO_4$ plume is explained by the combination of the presence of excess ammonia and stable meteorological conditions leading to building up and growth of aerosols [e.g., *Wang et al.*, 2011]. A visual inspection of IASI spectra over the polluted region confirmed the presence of emission signatures for $(NH_4)_2SO_4$, which demonstrates that the latter was emitted from the PBL. This is the first time that boundary layer aerosols are observed so clearly over this large polluted region.

By intercomparing all four species for CO polluted-only pixels, CO slightly correlates with SO_2 (correlation coefficient of 0.49), which indicates that these pollutants have some common sources such as coal combustion and also different sources. We find no correlation of NH_3 with the other primary species and only a very weak correlation (correlation coefficient of 0.11) with $(NH_4)_2SO_4$. The absence of correlation between primary pollutants clearly points to the different sources (agricultural for NH_3 and urban/industrial emissions for CO and SO_2). One possible explanation for the weak correlation between NH_3 and $(NH_4)_2SO_4$ could be the fast formation of the secondary aerosols when SO_2 and NH_3 rich air masses mix. The significant correlation between SO_2 and $(NH_4)_2SO_4$ (correlation coefficient of 0.51) suggests that SO_2 is depleted less quickly. Study of larger time periods and the combination with models would be needed to better characterize the transport and chemistry of the species in this region with various pollution sources.

The simultaneous detection of the different pollutants is possible for the event analyzed here not only because of the temperature inversion that increases sensitivity and enables concentrations to build up but also because of the low humidity, which is needed to detect SO_2 near the surface [*Bauduin et al.*, 2013]. These conditions are met in China almost exclusively in winter months. Considering this and a condition on thermal contrast, which typically needs to be larger than 6° in absolute value, we estimate that IASI would theoretically be able to capture large pollution episodes similar to the one discussed here in 10–15% of cases between November and March (30% if we take only January, February, and March). These statistics were performed using temperatures from the ECMWF reanalysis for 2011 and 2012 and considering a further 50% reduction of possible measurements due to the presence of cloud.

4. Summary

This study provides a detailed analysis of a severe pollution episode that occurred in the North China Plain in January 2013. We demonstrated for the first time that IASI is able to detect simultaneously a variety of anthropogenic pollutants (CO, SO_2, NH_3, and $(NH_4)_2SO_4$) in the China PBL when suitable meteorological conditions occur in winter. A recent study has demonstrated that multispectral (TIR/near-infrared) observations feature enhanced sensitivity to surface-level CO [*Worden et al.*, 2010]. Here we show that a TIR-only sounder is capable of measuring anthropogenic CO concentration down to the surface when both high levels of pollution and large negative thermal contrast are present. With the second IASI instrument launched on board MetOp-B in September 2012 (twice more data are now available), it will be possible to monitor pollution events of this type more accurately and more regularly. Also, with the improvement of retrieval algorithms and TIR satellite instruments, unprecedented opportunities will be offered to contribute to air quality evaluation and management.

Acknowledgments

IASI has been developed and built under the responsibility of the Centre National d'Etudes Spatiales (CNES, France). It is flown on board the MetOp satellites as part of the EUMETSAT Polar System. The IASI L1C and L2 data are received through the EUMETCast near real-time data distribution service. We thank Dorothée Coppens from EUMETSAT for her help in the course of the study. The authors acknowledge the French Ether atmospheric database (www.pole-ether.fr) for providing the IASI L1C data and L2 temperature data. The French scientists are grateful to CNES and Centre National de la Recherche Scientifique (CNRS) for financial support. S. Bauduin, L. Clarisse, and P.-F. Coheur are a Research Fellow, a Postdoctoral Researcher, and a Senior Research Associate (Chercheur Qualifié) with F.R.S.-FNRS, respectively. M. Van Damme is grateful to the "Fonds pour la Formation à la Recherche dans l'Industrie et dans l'Agriculture" of Belgium for a PhD grant (Boursier FRIA). The research in Belgium was funded by F.N.R.-FNRS; the Belgium State Federal Office for Scientific, Technical and Cultural Affairs; and the European Space Agency (ESA-Prodex arrangements). Financial support by the "Actions de Recherche Concertées" (Communauté Française de Belgique) is also acknowledged. The research also benefited from the activities undertaken in the frame of the Ozone and Atmospheric Composition Monitoring SAF and the ECLAIRE EU-FP7 project. The authors gratefully acknowledge the NOAA Air Resources Laboratory (ARL) for the provision of the HYSPLIT transport and dispersion model and/or READY website (www.arl.noaa.gov/ready.html) used in this publication. NCEP reanalysis data provided by the NOAA/OAR/ESRL PSD, Boulder, Colorado, USA, from their website at www.cdc.noaa.gov. We acknowledge ECMWF for the access to the meteorological data.

The Editor thanks two anonymous reviewers for their assistance in evaluating this paper.

References

Bauduin, S., L. Clarisse, D. Hurtmans, C. Clerbaux, and P.-F. Coheur (2013), Remote sensing of atmospheric boundary layer composition using IASI observations, paper presented at 3rd IASI Conference, EUMETSAT and CNES, Hyères, France. [Available at http://smsc.cnes.fr/IASI/presents_conf3.htm.]

Berrisford, P., D. Dee, K. Fielding, M. Fuentes, P. Kallberg, S. Kobayashi, and S. Uppala (2009), The ERA-Interim archive, *ERA Rep. Ser. 1*, ECMWF, Reading, U. K.

Bouwman, A. F., D. S. Lee, W. A. H. Asman, F. J. Dentener, K. W. Van Der Hoek, and J. G. J. Olivier (1997), A global high-resolution emission inventory for ammonia, *Global Biogeochem. Cycles*, *11*, 561–587.

Carboni, E., R. Grainger, J. Walker, A. Dudhia, and R. Siddans (2012), A new scheme for sulfur dioxide retrieval from IASI measurements: Application to the Eyjafjallajökull eruption of April and May 2010, *Atmos. Chem. Phys.*, *12*, 11,417–11,434.

Clarisse, L., M. W. Shephard, F. Dentener, D. Hurtmans, K. Cady-Pereira, F. Karagulian, M. Van Damme, C. Clerbaux, and P.-F. Coheur (2010), Satellite monitoring of ammonia: A case study of the San Joaquin Valley, *J. Geophys. Res.*, *115*, D13302, doi:10.1029/2009JD013291.

Clarisse, L., M. Fromm, Y. Ngadi, L. Emmons, C. Clerbaux, D. Hurtmans, and P.-F. Coheur (2011), Intercontinental transport of anthropogenic sulfur dioxide and other pollutants: An infrared remote sensing case study, *Geophys. Res. Lett.*, *38*, L19806, doi:10.1029/2011GL048976.

Clarisse, L., P.-F. Coheur, F. Prata, J. Hadji-Lazaro, D. Hurtmans, and C. Clerbaux (2013), A unified approach to infrared aerosol remote sensing and type specification, *Atmos. Chem. Phys.*, *13*, 2195–2221, doi:10.5194/acp-13-2195-2013.

Clerbaux, C., et al. (2009), Monitoring of atmospheric composition using the thermal infrared IASI/MetOp sounder, *Atmos. Chem. Phys.*, *9*, 6041–6054.

Dee, D., et al. (2011), The ERA-Interim reanalysis: Configuration and performance of the data assimilation system, *Q. J. R. Meteorol. Soc.*, *137*, 553–597, doi:10.1002/qj.828.

Deeter, M. N., D. P. Edwards, J. C. Gille, and J. R. Drummond (2007), Sensitivity of MOPITT observations to carbon monoxide in the lower troposphere, *J. Geophys. Res.*, *112*, D24306, doi:10.1029/2007JD008929.

Draxler, R. R., and G. D. Rolph (2014), HYSPLIT (HYbrid Single-Particle Lagrangian Integrated Trajectory) Model access via NOAA ARL READY Website (http://ready.arl.noaa.gov/HYSPLIT.php, NOAA Air Resources Laboratory, College Park, Md.

Edwards, D. P., et al. (2006), Satellite-observed pollution from Southern Hemisphere biomass burning, *J. Geophys. Res.*, *111*, D14312, doi:10.1029/2005JD006655.

Gao, H., J. Chen, B. Wang, S.-C. Tan, C. M. Lee, X. Yao, H. Yan, and J. Shi (2011), A study of air pollution of city clusters, *Atmos. Environ.*, *45*, 3069–3077, doi:10.1016/j.atmosenv.2011.03.018.

Hu, Z. (2009), Spatial analysis of MODIS aerosol optical depth, PM2.5, and chronic coronary heart disease, *Int. J. Health Geogr.*, *8*(27), doi:10.1186/1476-072X-8-27.

Huang, X., Y. Song, M. Li, J. Li, Q. Huo, X. Cai, T. Zhu, M. Hu, and H. Zhang (2012), A high-resolution ammonia emission inventory in China, *Global Biogeochem. Cycles*, *26*, GB1030, doi:10.1029/2011GB004161.

Hurtmans, D., P.-F. Coheur, C. Wespes, L. Clarisse, O. Scharf, C. Clerbaux, J. Hadji-Lazaro, M. George, and S. Turquety (2012), FORLI radiative transfer and retrieval code for IASI, *J. Quant. Spectros. Radiat. Transfer*, *113*, 1391–1408.

Lelieveld, J., and F. J. Dentener (2000), What controls tropospheric ozone?, *J. Geophys. Res.*, *105*, 3531–3551, doi:10.1029/1999JD901011.

Li, W., S. Zhou, X. Wang, Z. Xu, C. Yuan, Y. Yu, Q. Zhang, and W. Wang (2011), Integrated evaluation of aerosols from regional brown hazes over northern China in winter: Concentrations, sources, transformation, and mixing states, *J. Geophys. Res.*, *116*, D09301, doi:10.1029/2010JD015099.

Lin, W., X. Xu, B. Ge, and X. Liu (2011), Gaseous pollutants in Beijing urban area during the heating period 2007–2008: Variability, sources, meteorological, and chemical impacts, *Atmos. Chem. Phys.*, *11*, 8157–8170, doi:10.5194/acp-11-8157-2011.

Lin, W., X. Xu, Z. Ma, H. Zhao, X. Liu, and Y. Wang (2012), Characteristics and recent trends of sulfur dioxide at urban, rural, and background sites in north China: Effectiveness of control measures, *J. Environ. Sci.*, *24*(1), 34–49.

Liu, J., D. L. Mauzerall, and L. W. Horowitz (2008), Source-receptor relationships between East Asian sulfur dioxide emissions and Northern Hemisphere sulfate concentrations, *Atmos. Chem. Phys.*, *8*, 3721–3733, doi:10.5194/acp-8-3721-2008.

National Bureau of Statistics of China (2008), *China Statistical Yearbook 2008*, China Stat. Press, Beijing.

Rodgers, C. D. (2000), *Inverse Methods for Atmospheric Sounding: Theory and Practice, Series on Atmospheric, Oceanic and Planetary Physics*, World Sci., Hackensack, N. J.

Schwartz, S. E. (1989), Acid deposition: Unraveling a regional phenomenon, *Science*, *243*, 753–763.

Turquety, S., D. Hurtmans, J. Hadji-Lazaro, P.-F. Coheur, C. Clerbaux, D. Josset, and C. Tsamalis (2009), Tracking the emission and transport of pollution from wildfires using the IASI CO retrievals: Analysis of the summer 2007 Greek fires, *Atmos. Chem. Phys.*, *9*, 4897–4913, doi:10.5194/acp-9-4897-2009.

Van Damme, M., L. Clarisse, C. L. Heald, D. Hurtmans, Y. Ngadi, C. Clerbaux, A. J. Dolman, J. W. Erisman, and P. F. Coheur (2013), Global distributions and trends of atmospheric ammonia (NH3) from IASI satellite observations, *Atmos. Chem. Phys. Discuss.*, *13*, 24,301–24,342, doi:10.5194/acpd-13-24301-2013.

van Donkelaar, A., R. V. Martin, M. Brauer, R. Kahn, R. Levy, C. Verduzco, and P. J. Villeneuve (2010), Global estimates of ambient fine particulate matter concentrations from satellite-based aerosol optical depth: Development and application, *Environ. Health Perspect.*, *118*, 847–855, doi:10.1289/ehp.0901623.

Wang, L. T., Z. Wei, J. Yang, Y. Zhang, F. F. Zhang, J. Su, C. C. Meng, and Q. Zhang (2013), The 2013 severe haze over the southern Hebei, China: Model evaluation, source apportionment, and policy implications, *Atmos. Chem. Phys. Discuss.*, *13*, 28,395–28,451, doi:10.5194/acpd-13-28395-2013.

Wang, S., J. Xing, C. Jang, Y. Zhu, J. S. Fu, and J. Hao (2011), Impact assessment of ammonia emissions on inorganic aerosols in East China using response surface modeling technique, *Environ. Sci. Technol.*, *45*, 9293–9300.

Wang, T., A. Ding, J. Gao, and W. S. Wu (2006), Strong ozone production in urban plumes from Beijing, China, *Geophys. Res. Lett.*, *33*, L21806, doi:10.1029/2006GL027689.

Warneck, P. (2000), *Chemistry of the Natural Atmosphere*, 2nd ed., Academic, London.

Worden, H. M., M. N. Deeter, D. P. Edwards, J. C. Gille, J. R. Drummond, and P. Nédélec (2010), Observations of near-surface carbon monoxide from space using MOPITT multispectral retrievals, *J. Geophys. Res.*, *115*, D18314, doi:10.1029/2010JD014242.

Xu, W. Y., et al. (2011), Characteristics of pollutants and their correlation to meteorological conditions at a suburban site in the North China Plain, *Atmos. Chem. Phys.*, *11*, 4353–4369, doi:10.5194/acp-11-4353-2011.

Yang, K., R. R. Dickerson, S. A. Carn, C. Ge, and J. Wang (2013), First observations of SO_2 from the satellite Suomi NPP OMPS: Widespread air pollution events over China, *Geophys. Res. Lett.*, *40*, 4957–4962, doi:10.1002/grl.50952.

Zhang, X., J. van Geffen, H. Liao, P. Zhang, and S. Lou (2012), Spatiotemporal variations of tropospheric SO_2 over China by SCIAMACHY observations during 2004–2009, *Atmos. Environ.*, *60*, 1–9.

Zhang, Y. H., M. Hu, L. J. Zhong, A. Wiedensohler, S. C. Liu, M. O. Andreae, W. Wang, and S. J. Fan (2008), Regional integrated experiments on air quality over Pearl River Delta 2004 (PRIDE-PRD2004): Overview, *Atmos. Environ.*, *42*, 6157–6173.

Zhao, X. J., P. S. Zhao, J. Xu, W. Meng, W. W. Pu, F. Dong, D. He, and Q. F. Shi (2013), Analysis of a winter regional haze event and its formation mechanism in the North China Plain, *Atmos. Chem. Phys.*, *13*, 5685–5696, doi:10.5194/acp-13-5685-2013.